

Micromagnetic modelling of anisotropic damping in ferromagnet

Mykola Dvornik,* Arne Vansteenkiste, and Bartel Van Waeyenberge
DyNaMat Lab, Ghent University, Krijgslaan 281/S1, 9000 Ghent, Belgium

We report a numerical implementation of the Landau-Lifshitz-Baryakhtar theory, which dictates that the micromagnetic relaxation term obeys the symmetry of the magnetic crystal, i. e. replacing the single intrinsic damping constant with a tensor of corresponding symmetry. The effect of anisotropic relaxation is studied in thin saturated ferromagnetic disk and ellipse with and without uniaxial magneto-crystalline anisotropy. We investigate the angular dependency of the linewidth of magnonic resonances with respect to the given structure of the relaxation tensor. The simulations suggest that the anisotropy of the magnonic linewidth is determined by only two factors: the projection of the relaxation tensor onto the plane of precession and the ellipticity of the later.

Landau and Lifschitz¹ and later Gilbert^{2,3} introduced a phenomenological relaxation term in the equation of motion of magnetic moments in ferromagnetic media. They suggested that the magnetic losses are characterized by a single intrinsic damping constant of relativistic nature. Both the Landau-Lifshitz and the Gilbert phenomenological damping terms are essentially equivalent for low magnetic losses, while the Gilbert damping term works better for large values of the damping constant, as was pointed out by Kikuchi⁴. These terms are now widely used for the description of magnetic relaxations in magnetic thin films^{5,6} and patterned magnetic media⁷. The microscopic mechanism behind the magnetic losses has also been suggested, e.g. in Gilmore et al.⁸.

However, recent experimental data urges the development of new approaches to magnetic losses, i.e. by introducing higher order terms within Gilbert approach⁹, by introducing inert relaxation¹⁰ and by generalizing the magnetization dynamics and relaxation within the framework of Onsager's kinetic equations¹¹. The latter approach shows that the relaxation part of the equation of precession should obey the crystallographic symmetry of the media. Thereby replacing the single intrinsic damping constant with a tensor. The reason behind anisotropic relaxation in magnetic media is the symmetry properties of the spin-orbit and s-d interaction¹², which couple spins to other subsystems (i.e degrees of freedom), i.e. lattice and free electrons, respectively. The anisotropic character of these couplings results in anisotropic energy scattering from spins to other subsystems and vice-versa. It worth noting, that an angular dependency of magnetic losses (or effects associated with the same physics) have already been reported experimentally¹³⁻¹⁸. However analytical and numerical approaches still have to be developed, especially for nanoscale structures where magnetic resonances are strongly confined, and so, their spectra are discrete.

In this paper, we report on a numerical implementation of Baryakhtar theory within the mumax2 micromagnetic framework¹⁹. Furthermore, we systematically investigate the influence of the anisotropic relaxation on the the angular dependency of FMR linewidths in a nanoscale magnetic disk and ellipse.

We start from the general Baryakhtar equation (LLBr)

$$\frac{\partial \mathbf{M}}{\partial t} = -\gamma \mathbf{M} \times \mathbf{H} + \lambda_{ij}(M) H_j + \lambda_{ij,sp}^{(e)}(M) \frac{\partial^2 H_j}{\partial x_s \partial x_p} \quad (1)$$

where \mathbf{M} , γ , \mathbf{H} are the magnetization vector, gyromagnetic ratio and effective internal field respectively (having contributions from exchange, spin-orbit, Zeeman and magneto-static energies). λ and $\lambda^{(e)}$ are the relaxation tensors of relativistic and exchange nature, respectively, and in general are functions of the magnetization. It is worth noting, that in contrast to the Landau-Lifshitz formalism, the Baryakhtar equation does not conserve the length of the magnetization vector, i.e. $|\mathbf{M}| \neq \text{const.}$ However in the present study, we do not excite high-frequency (thermal) magnons and work in linear approximation only, so that the vibrations of magnetization vector length are negligible (although correctly accounted in our micromagnetic simulations).

For the sake of simplicity, this paper focuses on the lowest magnetic resonances (nearly uniform FMR) for which the second relaxation term in eq. (1) (of exchange nature) is vanishing, i.e. $\lambda^{(e)} \Delta \mathbf{H} \ll \lambda \mathbf{H}$. Such an assumption is reasonable since the majority of modern state-of-the-art experimental techniques have limited (if any) spatial resolution^{13,20}, and so, can only measure lowest magnonic resonances. In this case eq. (1) reduces to

$$\frac{\partial \mathbf{M}}{\partial t} = -\gamma \mathbf{M} \times \mathbf{H} + \lambda_{ij}(\mathbf{M}) H_j \quad (2)$$

The exact form of the relativistic tensor is unknown for an arbitrary magnetic configuration. However, the tensor can be expanded into the Taylor series in the vicinity of paramagnetic state ($\mathbf{M} = 0$)²¹, i. e. $\lambda_{ij}(\mathbf{M}) = \lambda_{ij}(0) + \mu_{ij,sp}(0) M_s M_p + \dots$, where λ_{ij} and μ_{sp} are first and second order relativistic relaxation tensors and s, p denote spatial components which are different from i, j . According to Ref.²¹, the first term in the expansion describe non-conservative relaxations, where energy dissipations is accompanied with angular momentum transfer. This mechanism dominates in ferromagnetic metals as become evident from experiments on ultra-fast demagnetisation²², therefore we omit higher order terms in Taylor expansion, so that $\lambda_{ij}(\mathbf{M}) = \lambda_{ij}(0)$. The latter expression could be

rewritten in terms of dimensionless damping tensor α_{ij} , i.e. $\lambda_{ij} = \gamma |\mathbf{M}| \mathbf{M} \times \alpha_{ij}$. So, finally eq. (2) transforms into

$$\frac{\partial \mathbf{M}}{\partial t} = -\gamma \mathbf{M} \times \mathbf{H} + \gamma M \alpha_{ij} \mathbf{H} \quad (3)$$

which under assumption of constant magnetisation length and isotropic relaxations transforms into well-known Landau-Lifshitz equation, $\frac{\partial \mathbf{M}}{\partial t} = -\gamma \mathbf{M} \times \mathbf{H} + \gamma M \alpha \mathbf{M} \times \mathbf{M} \times \mathbf{H}$. The eq. (3) is employed in the present study.

The simulations were carried on a thin magnetic disk and ellipse with equal thicknesses of 7 nm. The diameter of the disk is 110 nm, while ellipse has minor and major axes of 44 nm and 110 nm, respectively. The magnetic parameters are close to that of Cobalt, i.e. a saturation magnetization of $|\mathbf{M}| = M_s = 1440 \cdot 10^3$ A/m, exchange stiffness constant of $A_{ex} = 2.1 \cdot 10^{-11}$ J/m and uniaxial anisotropy strength of $K_u = 5.2 \cdot 10^5$ J/m³ (varying in some of the simulations). Cobalt has a hexagonal lattice for which the relaxation tensor is diagonal $\alpha_{ij} = \alpha \nu_{ij} \delta_{ij}$ ^{11,21}. For the sake of simplicity we show its diagonal elements as a vector. Cobalt is characterized by a relatively strong spin-orbit coupling, making it an ideal candidate for our case study and for possible experiments. The damping constant α is fixed to 0.008, while components of the tensor ν_{ij} are varied to mimic given magnetic configurations. In the present study, we only focus on the saturated case to depict the main features of anisotropic damping. For this purpose in all simulations we saturate the sample in-plane by using sufficiently large applied magnetic field of 1T.

The magnonic spectra are extracted by means of FFT from 40 ns time traces of the net magnetisation, simulated by exposing the relaxed magnetic states to a “sinc” excitation with an amplitude of 100 Oe and cut-off of 80 GHz. The bandwidth of the simulations is maintained at 100 GHz to avoid FFT aliasing. The magnetization dynamics always vanish within the time-frame of the simulation. So we would not expect any artificial broadening of the magnonic resonances. Nevertheless, the a windowing function is also applied before FFT to prevent spectral leakage.

The dominant peaks in the spectra (attributed to the magnonic resonances of different spatial characters) are fitted to Lorentzian curves in order to extract their amplitudes, frequencies ω and FWHM $\Delta\omega$. The latter two parameters are used to estimate the relative net relaxation rates given by the Landau-Lifshits-Baryakhtar and Landau-Lifshits models as $\Gamma_{LLBr} = \Delta\omega_{LLBr}/\omega_{LLBr}$ and $\Gamma_{LLG} = \Delta\omega_{LLG}/\omega_{LLG}$, respectively. Finally, the ratio between two is calculated as $\eta = \Gamma_{LLBr}/\Gamma_{LLG}$ to estimate the difference in two micromagnetic models.

The spatial profiles of the magnonic modes are calculated using the method from Ref.²³. The typical spectra and spatial profiles of the modes are shown in Fig. 1. For the disk, we excite two dominant modes of “edge” (lowest magnonic mode) and “bulk” (higher order magnonic mode) character for any direction of saturation

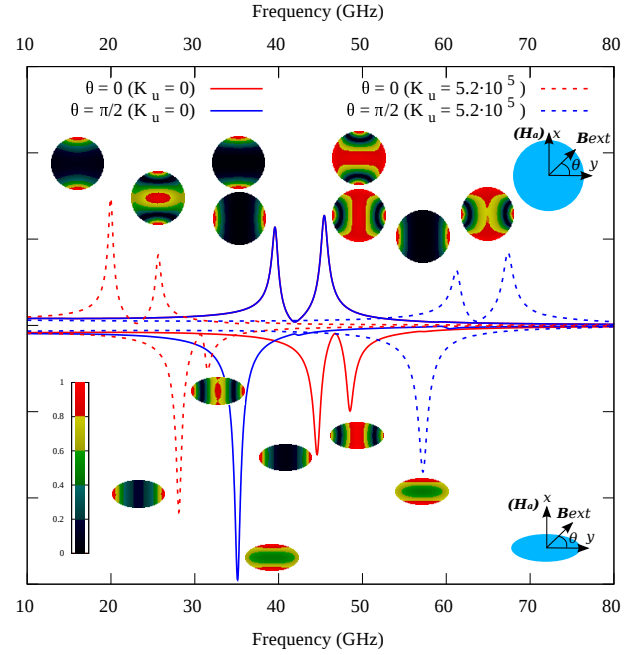


Figure 1: The spectra of magnonic resonance and corresponding spatial mode profiles are shown for disk (top panel) and ellipse (bottom panel). The solid and dashed lines correspond to the isotropic and uniaxial materials, respectively.

(within $[0, \pi/2]$). In contrast, for an ellipse only the edge mode remains within the frequency bandwidth of simulations for all directions of saturation. The bulk mode is rendered above 80 GHz due to enhanced contribution of exchange energy when magnetised along minor axis. The uniaxial anisotropy acts as expected from trivial physical considerations²⁴, i. e. hardening (softening) magnonic resonances for the parallel (perpendicular) configurations, respectively.

The anisotropy of magnonic damping has never been measured qualitatively. Since the aim of this paper is to show its effect on magnetisation dynamics, the degree of anisotropy is chosen to make sure that simulations are both computationally feasible and numerically stable. So in all following cases, the anisotropy

of damping is represented by reducing given components of the relaxation tensor by one order of magnitude. However, Baryakhtar showed that components of the relaxation tensor could be expressed in terms of magneto-crystalline anisotropy constants²¹. So the damping should be isotropic, when there is no magneto-crystalline anisotropy present. For demonstration purposes we vary it nevertheless in this study. Furthermore, in the simulations where anisotropy constant is varied, the corresponding components of the damping tensor remain constant to draw straight comparison between LLG and LLBr models. More rigorous treatment is expected to change our results quantitatively, but not qualitatively.

The angular dependency of the relative macroscopic damping constant for different structures of the tensor

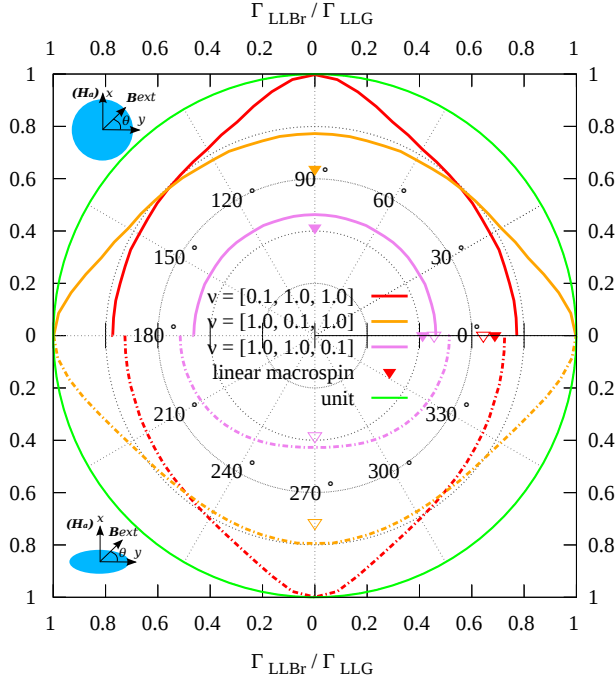


Figure 2: The angular dependency of the ratio between net relaxation rates of LLBr and LLG is shown for different structures of damping tensor, ν_{ii} . The ratio is extracted for the edge mode in isotropic Co nano-element ($K_u = 0 \text{ Jm}^{-3}$). The top $(0, \pi)$ and bottom $(\pi, 2\pi)$ semi-planes correspond to the disk and ellipse, respectively.

ν_{ii} is shown in Fig. 2 for an isotropic Co disk (top panel) and ellipse (bottom panel). First of all, the symmetry of the graph is two-fold and mimics that of the relaxation tensor. Secondly, the data suggests that changes of the relaxation constant along saturation direction do not change the value of the macroscopic damping constant with respect to the one obtained from LLG, i.e. $\eta_0^{0.1,1,1} = \eta_{\pi/2}^{0.1,1,1} \approx 1$, where top and bottom indices show diagonal elements of the relaxation tensor and angle of saturation respectively. Meanwhile, when the components of the relaxation tensor are reduced orthogonally to the saturation direction, a distinct reduction of relative relaxation rate is observed, i.e. $\eta_0^{0.1,1,1} = \eta_{\pi/2}^{1,0,1} \approx 0.77$ and $\eta_0^{0.1,1,1} \approx 0.73$, $\eta_{\pi/2}^{1,0,1} \approx 0.79$, for the disk and ellipse, respectively. Finally, for the case of reduced out-of-plane component of relaxation tensor, $\nu_{ii} = (1, 1, 0.1)$, the relative macroscopic damping is always reduced below the value observed for the in-plane case, i.e. $\eta_0^{1,1,0.1} = \eta_{\pi/2}^{1,1,0.1} \approx 0.46$ and $\eta_0^{1,1,0.1} \approx 0.51$, $\eta_{\pi/2}^{1,1,0.1} \approx 0.43$, for disk and ellipse respectively. So when the relaxation tensor is uniform in-plane, the relative relaxation rate in the disk is independent on the direction of saturation as it follows from its rotational symmetry. In contrast, for the ellipse the symmetry is two-fold, so not only the relaxation tensor contributes to the symmetry of the magnonic damping.

In general, the magnetisation vector has three degrees

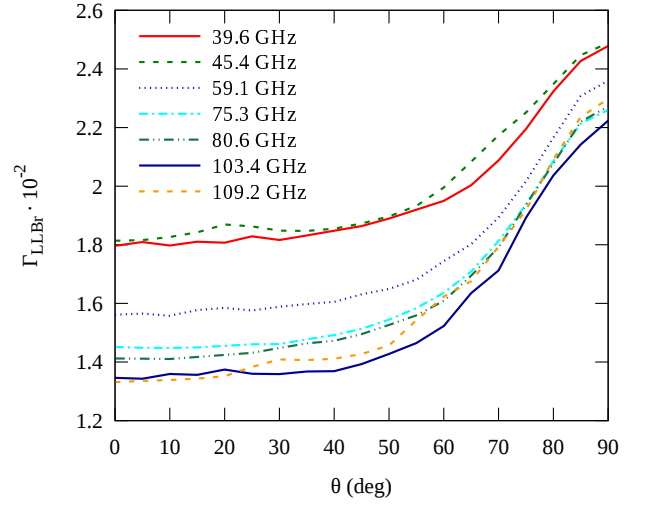


Figure 3: The angular dependency of relative relaxation rate of different magnonic modes in isotropic Co disk ($K_u = 0 \text{ Jm}^{-3}$). is shown. The value of the relaxation tensor is $\nu_{ii} = [0.1, 1, 1]$. The numbers in the key represent frequencies of the modes expressed in GHz.

of freedom. Two of them correspond to precession (transverse degrees of freedom) and one corresponds to the changes of the vector's length (longitudinal degree of freedom). In linear approximation, the longitudinal degree of freedom is "frozen", so that it does not dissipate energy. It explains why there are no changes observed between LLBr and LLG, when the relaxation tensor is altered along the longitudinal direction. Linearisation of the LLBr equation in the macrospin approximation under assumption of diagonal relaxation tensor leads to

$$\Gamma \sim \nu_{ii} \frac{\omega_i}{\omega} = \nu_{ii} \sqrt{\frac{\omega_i}{\omega_j}} \quad (4)$$

The frequency of the precession is given by $\omega^2 = \omega_i \omega_j$, $i \neq j$, ω_i and ω_j are characteristic frequencies of transversal degrees of freedom. Eq.(4) has clear physical meaning, so that the amount of dissipated energy is proportional to the energy stored in all degrees of freedom. So the striking difference between relaxation rates, i. e. $\eta_0^{0.1,1,1}/\eta_{\pi/2}^{1,1,0.1} = 1.67$ and $\eta_0^{0.1,1,1}/\eta_0^{1,1,0.1} = 1.59$ and $\eta_{\pi/2}^{1,0,1}/\eta_{\pi/2}^{1,1,0.1} = 1.84$, suggest that for the given magnonic mode the out-of-plane degree of freedom stores more energy, than in-plane. So by estimating the ratio between the relaxation rates Γ/Γ' for the different structures of the damping tensor ν and ν' , it is possible to find the characteristic frequency of different degrees of freedom. In particular, for the out-of-plane component it reads:

$$\omega_z = \sqrt{\frac{\nu_{ii} - (\Gamma/\Gamma')\nu'_{ii}}{(\Gamma/\Gamma')\nu'_{zz} - \nu_{zz}}} \omega, \quad i = x, y \quad (5)$$

If our assumption is valid, then for the disk the frequency

should be independent of the direction of in-plane saturation. For the lowest magnonic mode, the simulated relaxation rates for $\nu_{ii} = [0.1, 1, 1]$ and $\nu'_{ii} = [1, 1, 0.1]$, lead to the values of ω_z of ≈ 54.26 GHz and ≈ 47.94 GHz, at 0 rad and $\frac{\pi}{2}$ rad, respectively. For the higher order magnonic mode, the values of ω_z at 0 rad and $\frac{\pi}{2}$ rad are ≈ 62.54 GHz and ≈ 55.54 GHz, respectively.

The relative difference of $\frac{\omega_z(0) - \omega_z(\pi/2)}{\omega_z(0)} \approx 11.2\%$ between the values of ω_z at 0 rad and $\frac{\pi}{2}$ rad is roughly the same for these two modes, suggesting presence of damping mechanism beyond trivial linear macrospin model. The calculated angular dependency cannot be simply attributed to the artificial edge roughness (and corresponding two-magnon scattering relaxation mechanism), because “bulk” modes are not sensitive to it²⁵. So we assume that the observed discrepancy is due to the excitation of the second harmonics in the longitudinal degree of freedom. According to the simulations, the ratios between the amplitudes of the second harmonics and corresponding eigen modes are around 10^{-3} . This dissipation channel is not accounted in our simple model.

The analysis suggests that for the “edge” and “bulk” modes of the disk, the out-of-plane characteristic frequencies are much larger than the in-plane, $\omega_z \gg \omega_y$. The ratio between the characteristic frequencies could be controlled by various types of anisotropy, e.g. magneto-crystalline and shape anisotropies. Moreover, the ratio between the ω_z and ω_y might change for the higher-order modes because of interplay of shape anisotropy and exchange energies as explained in Ref.²⁶. In particular, in thin magnetic nano-elements $\omega_y/\omega_z \ll 1$ and $\omega_y/\omega_z \rightarrow 1$ for low- and high-frequency magnons, respectively. Therefore we can expect that the relaxation rate is mode specific. The relative relaxation rate, Γ_{LLBr} , for different magnonic modes of the isotropic disk with $\nu_{ii} = [0.1, 1, 1]$ is presented in Fig. 3. The relative linewidth decreases with the frequency of the mode as we expected. So for the higher order magnons the in-plane characteristic frequency tends to out-of-plane, thereby equalizing both relaxation channels. So for high frequency magnons the relaxation rate eventually approaches the limit defined by the components of the relaxation tensor, i.e. 0.0044 and 0.008 for $\theta = 0$ and $\theta = \pi/2$, respectively. The calculated values of the relaxation rate are somewhat higher than the intrinsic values fixed by the relaxation tensor. This can be attributed to the non-uniform spatial character of the magnonic modes²⁷.

Lets us employ this formalism to explain the results obtained in an ellipse, which naturally introduces an in-plane shape anisotropy. For the cases of $\nu_{ii} = [0.1, 1, 1]$ at 0 rad (along minor axis) and $\nu_{ii} = [1, 0.1, 1]$ at $\frac{\pi}{2}$ rad (along major axis) the in-plane and out-of-plane characteristic frequencies are $\omega_x \approx 36.14$ GHz, $\omega_z \approx 55.11$ GHz and $\omega_y \approx 23.81$ GHz, $\omega_z \approx 51.11$ GHz, respectively. For both cases the ω_z is similar to that of the disk, while the in-plane characteristic frequency is enhanced (reduced) for saturation along major (minor) axis. The latter is expected for in-plane shape anisotropy²⁸. For the quant-

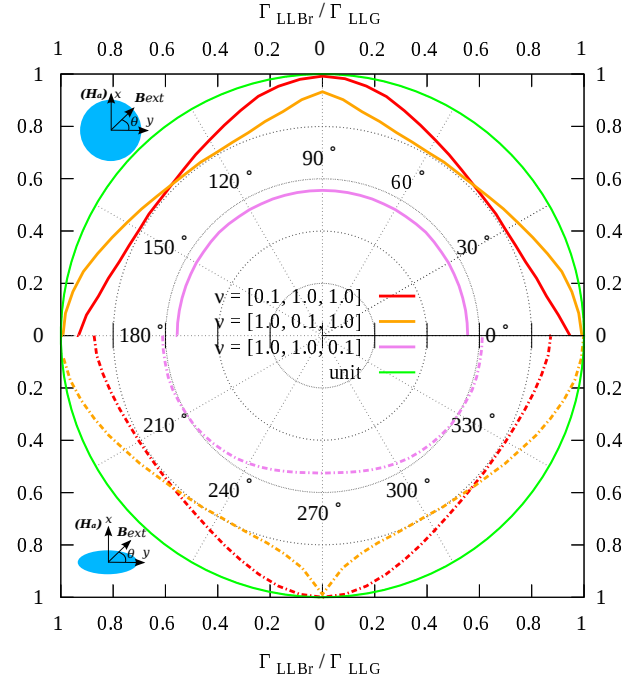


Figure 4: The angular dependency of the ratio between net relaxation rates of LLBr and LLG is shown for different structures of damping tensor, ν_{ii} . The ratio is extracted for the edge mode in uniaxial Co nano-element ($K_u = 5.2 \cdot 10^5$ Jm⁻³). The top (0, π) and bottom (π , 2π) semi-planes correspond to the disk and ellipse, respectively.

ity represented in Fig. 2 we can simply write:

$$\eta = \frac{\Gamma_{LLBr}}{\Gamma_{LLG}} = \frac{1}{1 + \omega_z/\omega_i} \nu_{ii} + \frac{1}{1 + \omega_i/\omega_z} \nu_{zz}, \quad (6)$$

where $i = x, y$ for 0 rad and $\frac{\pi}{2}$ rad respectively. These theoretical values are given by dots in Fig. 2. The theory qualitatively mimics the behaviour observed in Fig. 2, further supporting our linear model of anisotropic magnonic relaxation.

In contrast to shape, magneto-crystalline anisotropy could be easily introduced and tuned. The relative linewidth calculated on the same samples, but in the presence of uniaxial anisotropy is shown in Fig. 4. The direction of uniaxial anisotropy always coincides with the shortest eigenvector of the damping tensor for the reasons explained above. The results presented in Fig. 4 qualitatively reproduce those from Fig. 2. For all the cases at 0 ($\frac{\pi}{2}$) rad the uniaxial anisotropy softens (hardens) lowest magnonic mode. Thus, reducing (enhancing) influence of in-plane relaxation. Therefore the relative relaxation rate is always enhanced as compared to anisotropy-less case. Furthermore, in case of ellipse for $\nu_{ii} = [1, 0.1, 1]$ at $\frac{\pi}{2}$ rad the relative linewidth tends to unity. The effect could be easily explained if we take into account that shape and uniaxial anisotropies act in the same way, i.e. soften the lowest magnonic mode, eventually vanishing the role of in-plane relaxation. Since out-of-plane relax-

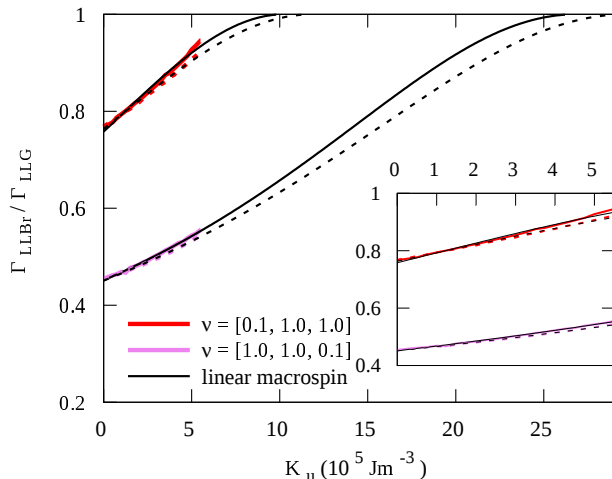


Figure 5: The relative magnonic resonance linewidth $\Gamma_{LLBr}/\Gamma_{LLG}$ in function of uniaxial anisotropy constant K_u is shown for different structures of the relativistic relaxation tensor $\alpha\nu_{ii}$. The solid and dotted lines correspond to the “edge” and “bulk” modes of uniaxial Co disk, respectively. As we increase the uniaxial anisotropy constant, the relaxation rate calculated with LLBr tends to that of LLG.

ation is equal to that of isotropic case, the linewidth also tends to that of isotropic case.

So, by tuning the strength of the uniaxial anisotropy we can effectively change the relaxation rate within the limits defined by the anisotropy of damping tensor. The relative linewidth as a function of uniaxial anisotropy constant, K_u , is shown in Fig. 5. The fit to our simple model is also shown. We assumed that the frequency of the mode is given by (SI units):

$$\omega = \omega_0 - \frac{(\gamma/2\pi)}{\mu_0 M_s} K_u \quad (7)$$

where ω_0 is the frequency of the mode in isotropic case with the assumption that contribution of the anisotropy energy is second order with respect to ω_0 . So the relative relaxation rate is given by:

$$\eta = \frac{1}{1 + (\omega_j/\omega)^2 \nu_{ii}} + \frac{1}{1 + (\omega/\omega_j)^2 \nu_{jj}} \quad (8)$$

The relative linewidth increases with the strength of uniaxial anisotropy and tends to unity, as it seen from our model. In particular, for the given case of the the anisotropy axis parallel to either in-plane or out-of-plane degrees of freedom, the mode frequency (and so corresponding characteristic frequency) is reduced as compared to the isotropic case. Thereby reducing the influence of relaxations along the anisotropy axis (the one which is reduced as compared to LLG). Therefore, as the the strength of the anisotropy increases, the relaxation rate tends to that of the LLG. The significant difference between the slopes in Fig. 5 is due to the difference in characteristic frequencies as it follows from eq. 6.

Based on our model and results obtained in isotropic disk and ellipse we conclude that (a) the highest reduction of relaxation rate is observed when the shortest eigen vector of the relaxation tensor is parallel to the hardest degree of freedom and (b) reduction of characteristic frequency leads to the reduction of corresponding relative relaxation rate. These conclusions could be used to design a representative experiment, e.g. measurements of magnonic linewidths in Co nano-elements with in-plane and out-of-plane uniaxial anisotropies. Then by estimating the characteristic frequencies from the micromagnetic simulations, the corresponding components of the relaxation tensor could be extracted.

We showed that anisotropic nature of the relaxation constant leads to a corresponding anisotropy in the linewidth of magnonic resonances. We showed that magnonic relaxation rate is mode specific even if the relaxation tensor is uniform. The strength of the effect depends on the ratio between the characteristic frequencies of transverse degrees of freedom of magnetization. The introduction of anisotropic damping makes this effect even more prominent. We showed that the relaxation rate could be altered by changing the strength of the magneto-crystalline anisotropy. We suggest that the latter effect could be experimentally verified in multi-ferroic materials. Finally, our numerical implementation is open, and so, it can be freely used by the community to fit experimental data.

* Electronic address: Mykola.Dvornik@ugent.be;
URL: <http://dynamat.ugent.be>

¹ L. D. Landau and E. Lifschitz, Phys. Z. Sowjetunion **8**, 153 (1935).

² T. Gilbert, Phys. Rev. **100**, 1236 (1955).

³ T. Gilbert, IEEE Trans. Magn. **40**, 3443 (2004).

⁴ R. Kikuchi, J. Appl. Phys. **27**, 1352 (1956).

⁵ H. Yu, R. Huber, T. Schwarze, F. Brandl, T. Rapp, P. Berberich, G. Duerr, and D. Grundler, Appl. Phys. Lett. **100**, 262412 (2012).

⁶ X. Joyeux, T. Devolder, J. V. Kim, Y. G. de la Torre, S. Eimer, and C. Chappert, J. Appl. Phys. **110**, 063915 (2011).

⁷ V. V. Kruglyak, S. O. Demokritov, and D. Grundler, J. Phys. D: Appl. Phys. **43**, 260301 (2010).

⁸ K. Gilmore, Y. U. Idzerda, and M. D. Stiles, Phys. Rev. Lett. **99**, 027204 (2007).

⁹ V. Tiberkevich and A. Slavin, Phys. Rev. B **75**, 014440 (2007).

¹⁰ M. Fahnle, D. Steiauf, and C. Illg,

- Phys. Rev. B **84**, 172403 (2011).
- ¹¹ I. V. Baryakhtar and V. Baryakhtar, Ukr. Phys. Journ. **43**, 1433 (1998).
 - ¹² V. Heine, Phys. Rev. **153**, 673 (1967).
 - ¹³ P. S. Keatley, P. Gangmei, M. Dvornik, R. J. Hicken, J. R. Childress, and J. A. Katine, Appl. Phys. Lett. **98**, 082506 (2011).
 - ¹⁴ S. Serrano-Guisan, K. Rott, G. Reiss, and H. W. Schumacher, J. Phys. D: Appl. Phys. **41**, 164015 (2008).
 - ¹⁵ H. W. Schumacher, S. Serrano-Guisan, K. Rott, and G. Reiss, Appl. Phys. Lett. **90**, 042504 (2007).
 - ¹⁶ S. Mizukami, Y. Ando, and T. Miyazaki, Jpn. J. Appl. Phys. **40**, 580 (2000).
 - ¹⁷ M. L. Schneider, J. M. Shaw, A. B. Kos, T. Gerrits, T. J. Silva, and R. D. McMichael, J. Appl. Phys. **102**, 103909 (2007).
 - ¹⁸ M. Buchmeier, D. E. Bürgler, P. A. Grünberg, C. M. Schneider, R. Meijers, R. Calarco, C. Raeder, and M. Farle, Phys. Stat. Sol. (a) **203**, 1567 (2006).
 - ¹⁹ A. Vansteenkiste and B. Van de Wiele, J. Magn. Magn. Mater. **323**, 2585 (2011).
 - ²⁰ K. Perzlmaier, M. Buess, C. H. Back, V. E. Demidov, B. Hillebrands, and S. O. Demokritov, Phys. Rev. Lett. **94**, 057202 (2005).
 - ²¹ V. G. Bar'yakhtar and A. G. Danilevich, Low Temp. Phys. **36**, 303 (2010).
 - ²² B. Koopmans, G. Malinowski, F. Dalla Longa, D. Steiauf, M. Fahnle, T. Roth, M. Cinchetti, and M. Aeschlimann, Nat. Mater. **9**, 259 (2010).
 - ²³ M. Dvornik, P. V. Bondarenko, B. A. Ivanov, and V. V. Kruglyak, J. Appl. Phys. **109**, 07B912 (2011).
 - ²⁴ P. A. G. Gurevich and G. Melkov, *Magnetization Oscillations and Waves* (CRC Press, 1996).
 - ²⁵ B. B. Maranville, R. D. McMichael, S. A. Kim, W. L. Johnson, C. A. Ross, and J. Y. Cheng, J. Appl. Phys. **99**, 08C703 (2006).
 - ²⁶ M. Dvornik and V. V. Kruglyak, Phys. Rev. B **84**, 140405 (2011).
 - ²⁷ B. Hillebrands and K. Ounadjela, *Topics in Applied Physics* (Springer, 2010) p. 23.
 - ²⁸ M. Pardavi-Horvath, B. G. Ng, F. J. Castano, H. S. Körner, C. Garcia, and C. A. Ross, J. Appl. Phys. **110**, 053921 (2011).